Industrial Chemistry & Materials

ROYAL SOCIETY OF CHEMISTRY

PAPER

View Article Online
View Journal | View Issue

Cite this: *Ind. Chem. Mater.*, 2025, **3**, 353

Enhanced lithium extraction from brine using surface-modified $LiMn_2O_4$ electrode with nanoparticle islands†

Guiling Luo,[a] Muyao He,[b] Li Zhang,[b] Jianquan Deng,[a] Linlin Chen,[c] Yanhong Chao,*[b] Haiyan Liu,[a] Wenshuai Zhu *[a] and Zhichang Liu[a]

Lithium is an important raw material for new energy-powered vehicles, and ensuring its supply is of great significance for global green and sustainable development. Salt lake brine is the main lithium resource, but the separation of Li^+ from coexisting metals poses a major challenge. In this work, a lithium-storing metal oxide SnO_2 nanoparticle island-modified $LiMn_2O_4$ electrode material is designed to endow $LiMn_2O_4$ with higher lithium extraction capacity and cycling stability. The SnO_2 nanoparticle islands effectively mitigate stress during the charge–discharge process of $LiMn_2O_4$, thereby enhancing cycling stability and promoting the diffusion of Li^+. The lithium adsorption capacity of the $LiMn_2O_4$ electrode material modified with SnO_2 nanoparticles reaches 19.76 mg g^{-1} within 1 hour, which is 1.7 times higher than that of $LiMn_2O_4$ (11.45 mg g^{-1}). The $LiMn_2O_4$ electrode material modified with SnO_2 nanoparticles shows good selectivity and cycling stability for the separation of lithium ions.

Received 24th December 2024,
Accepted 27th January 2025

DOI: 10.1039/d4im00159a

rsc.li/icm

Keywords: Electrochemical adsorption; Extraction lithium; Surface modified; $LiMn_2O_4$.

1 Introduction

The increasing demand for lithium, primarily driven by the proliferation of lithium-ion batteries, is expected to result in a significant supply shortage by 2030.[1,2] Lithium resources include continental brines, geothermal brines, seawater, lithium spodumene, lithium montmorillonite, lithium feldspar, and lithium mica, with China's salt lake brine reserves accounting for 80% of the global reserves.[3–5] To address this impending imbalance, extracting lithium from salt lake brines has emerged as a highly promising strategy.[6,7] Salt lake lithium extraction can partially replace lithium extraction from solid-state ores, reducing reliance on imported ores and reducing energy consumption and carbon emissions.[8–10] Electrochemical methods for lithium extraction from salt lake brines are particularly advantageous due to their simplicity, high recovery efficiency, and cost-effectiveness.[11,12] By leveraging these methods, it is possible to enhance the sustainability of lithium production, ensuring a more stable supply chain and contributing to the reduction of energy consumption and carbon emissions in the process.

Electrochemical methods involve applying a certain strength of electric field to assist the selective capture/release of Li^+ on electrode materials, enabling the extraction and enrichment of Li^+ from the mixed solution phase.[13,14] $LiMn_2O_4$ (LMO), is widely used as electrode materials for selective Li^+ capture, attributed to the spinel-type LMO having specific lithium vacancies and appropriate potential windows, resulting in excellent Li^+ selectivity.[15,16] The selectivity of LMO for Li^+ is primarily influenced by the size difference between Li^+ and other cations present in the solution.[17,18] The ionic radii of common cations found in salt lakes are as follows: Mg^{2+} (0.072 nm), Li^+ (0.076 nm), Na^+ (0.102 nm), Ca^{2+} (0.106 nm), and K^+ (0.138 nm).[19,20] While LMO can selectively insert and extract Li^+, the similar size of Mg^{2+} poses a challenge for exclusive Li^+ recovery based solely on ionic radius. Studies have shown that solvation radius is related to the transport in aqueous solutions, the difference in hydration energy between these ions significantly aids in selective extraction.[21,22] Mg^{2+} has a much higher hydration energy (1922 kJ mol^{-1}) compared to Li^+ (515 kJ mol^{-1}), which, combined with the synergy between the hydrated ion radius and the ion radius, enhances the selective extraction mechanism for Li^+.[23] This combination of factors

[a] College of Chemical Engineering and Environment, State Key Laboratory of Heavy Oil Processing, China University of Petroleum-Beijing, Beijing 102249, China. E-mail: zhuws@cup.edu.cn
[b] College of Science, State Key Laboratory of Heavy Oil Processing, China University of Petroleum-Beijing, Beijing 102249, China. E-mail: chaoyh@cup.edu.cn
[c] School of Chemistry and Chemical Engineering, Jiangsu University, Zhenjiang 212013, Jiangsu, China

† Electronic supplementary information (ESI) available. See DOI: https://doi.org/10.1039/d4im00159a

makes LMO-based electrochemical methods effective for lithium recovery.

However, the inherent properties of LMO determine its poor cycling stability, and there is a gap between the actual lithium extraction capacity and the theoretical capacity, limiting its application in electrochemistry. Surface coating, doping, and core–shell structures are common techniques for modifying LMO electrodes, each with distinct advantages and limitations. Surface coatings improve cycling stability by suppressing side reactions and Mn dissolution but can hinder lithium-ion transport if not uniformly applied.[24,25] Doping stabilizes the crystal structure and enhances conductivity; however, excessive doping can disrupt the spinel structure and reduce performance.[26] Core–shell structures offer structural stability and surface protection but face challenges with synthesis complexity, scalability, and lithium-ion transport across interfaces.[27] Surface modification of metal oxides is an effective method to improve surface chemical stability, resist stresses during charge and discharge processes, and inhibit the Jahn–Teller effect of LMO.[28–30] In recent years, lithium storage anodes prepared using metal oxide materials such as TiO_2, SnO_2, and Fe_2O_3 have attracted considerable attention due to their high chemical stability and reversible capacity.[31–33] SnO_2 nanoparticles exhibit excellent Li^+ storage capability, with a theoretical Li^+ storage capacity of up to 740 mAh g^{-1}.[34] The SnO_2 nanoparticle island modification approach stands out by offering a uniform and scalable method to enhance the cycling stability of LMO electrodes while suppressing Mn dissolution during charge–discharge cycles.[35] The nanoparticle islands effectively mitigate structural stress, ensuring better long-term stability compared to conventional surface coatings or core–shell structures.[36] Additionally, SnO_2 possesses high thermal stability and oxidation resistance, is insoluble in water, and is also difficult to dissolve in acidic or alkaline solutions, making it suitable for various aqueous environments.

Herein, this work designed and synthesized LMO electrode materials modified with SnO_2 nanoparticles with high lithium capacity and chemical surface stability, and constructed an electrochemical lithium extraction system from brine. The physical and chemical properties of samples were systematically characterized using SEM, TEM, HRTEM, Raman, XRD, XPS, and other techniques. The electrochemical quasi *in situ* spectroscopy characterization elucidated the deintercalation mechanism of Li^+ in the SnO_2 nanoparticle-modified LMO (SnLMO) structure, and the XRD spectra of the material after cycling clarified the influence of SnLMO on the Jahn–Teller effect. In addition, the effects of interfering ions on the electrode polarization of SnLMO, extraction capacity and cycling stability of lithium were also investigated.

2 Results and discussion

2.1 Structure and morphology

The surface of LMO is smooth and presents a truncated octahedral morphology (Fig. 1a). The particle size follows a

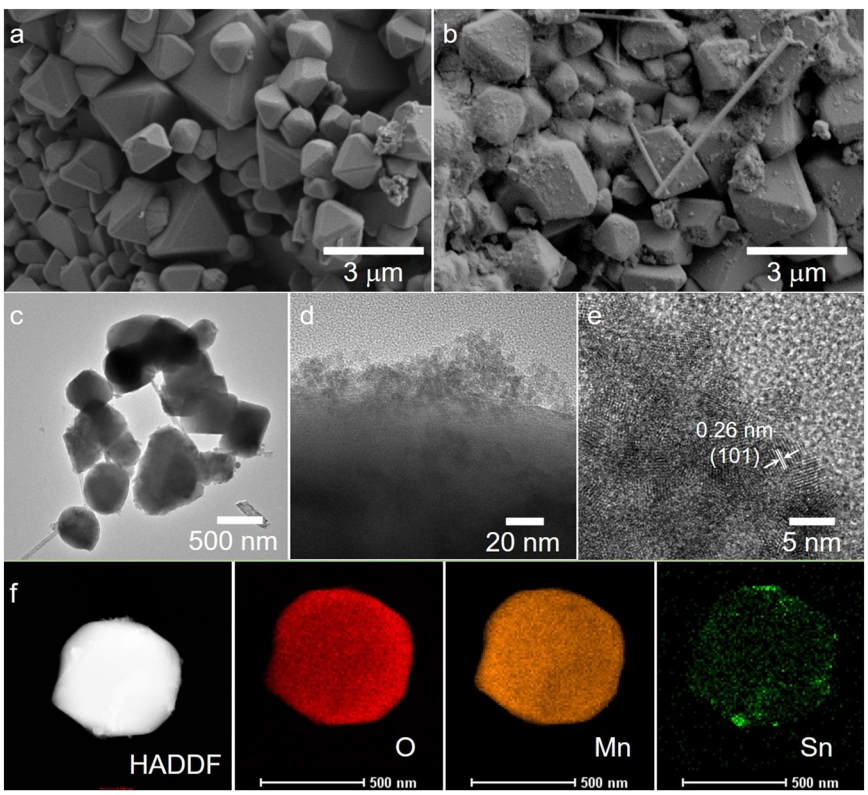

Fig. 1 SEM images of LMO (a) and SnLMO-1 (b); TEM (c and d), HRTEM (e), mapping (f) images of SnLMO-1.

normal distribution with an average of 570 ± 20 nm (Fig. S1†), and there are a few large particles exceeding 2 μm. SnLMO-1 exhibits a truncated octahedral morphology with uniformly attached agglomerated nanoscale particles on the surface, with very few nanowires present (Fig. 1b). TEM images of SnLMO-1 indicate that SnO_2 nanoparticles are uniformly loaded onto the surface of LMO, with a small amount of nanowires present (Fig. 1c and d). From the HRTEM image (Fig. 1e), it is evident that the SnO_2 nanoparticles on SnLMO-1 possess a clear lattice structure with a lattice size of 0.26 nm, belonging to the (101) plane.[33] EDX elemental analysis and mapping results demonstrate the uniform distribution of Sn elements on the surface of lithium manganese oxide (Fig. 1f and S2†). Furthermore, with increasing loading amounts, SnLMO-2 and SnLMO-3 exhibit a higher density of nanowires without altering the basic morphology of the truncated octahedron (Fig. S3 and S4†). In LMO materials loaded with SnO_2 nanowires, clear lattice fringes of the SnO_2 (110) plane are observed, with a lattice size of 0.31 nm (Fig. S5†).

The characteristic peaks in the XPS spectrum of Mn^{3+} and Mn^{4+} (Mn $2p^{3/2}$ and Mn $2p^{1/2}$) in LMO are located at 640.1, 651.6 eV and 641.5, 653.0 eV, respectively; with proportions of 42.28% and 57.72%, respectively (Fig. 2a). After being modified with 0.5 wt% SnO_2, the binding energies of Mn^{3+} and Mn^{4+} are shifted, with characteristic peak positions at 640.4, 651.8 eV and 641.9, 653.1 eV, respectively; with proportions of 53.06% and 46.94%, respectively. The O 1s peaks of LMO are located at 528.5, 529.8, and 531.4 eV, corresponding to lattice oxygen, Mn–O, and surface physically adsorbed water molecules O–H,[30,37] respectively; with proportions of 16.60%, 31.93%, and 51.47%, respectively. The O 1s peaks of SnLMO-1 are located at 528.3, 530.4, and 532.2 eV, corresponding to lattice oxygen, Mn–O, and surface physically adsorbed water molecules O–H, respectively; with proportions of 23.52%, 29.22%, and 47.26%, respectively (Fig. 2b). The characteristic peaks at 493.5 eV and 485.1 eV are attributed to Sn $3d^{3/2}$ and Sn $3d^{5/2}$, respectively (Fig. 2c), indicating the successful modification of Sn on LMO.[38] The presence of SnO_2 enhances the binding energy of LMO, improving surface stability.[39] XRD spectra show consistent characteristic peaks for LMO and SnLMO, with no shift in characteristic peaks with increasing modification, indicating that the internal crystal structure of LMO remains unchanged after being modified with SnO_2 (Fig. 2d). There are also no characteristic peaks of SnO_2 appearing after modification, possibly due to the low modified amount or uniform distribution of the modified.

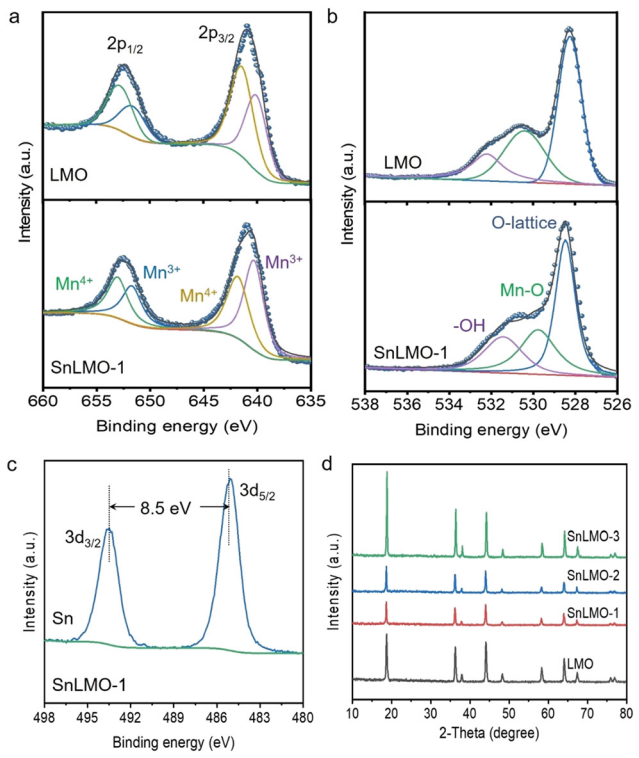

Fig. 2 High-resolution XPS spectra of Mn 2p (a), O 1s (b), and Sn 3d (c) of LMO and SnLMO-1; XRD patterns (d) of LMO and SnLMO.

2.2 Electrochemical selectivity and dynamics

2.2.1 Electrochemical selectivity. Selectivity is an important indicator for evaluating electrochemical systems for lithium recovery from salt lakes. The preliminary investigation of Li^+ selectivity is typically conducted using cyclic voltammetry, followed by further evaluation of the overpotential generated by interfering cations using constant current discharge curves. The test curves of SnLMO-1 in different electrolyte solutions were obtained using cyclic voltammetry (Fig. 3a) and the constant current discharge method (Fig. 3b). In solutions containing Li^+, two pairs of redox peaks can be observed. The redox peaks at this potential can be attributed to the redox potential of $Mn^{3+/4+}$, which is accompanied by the release and capture of lithium process. In contrast, in solutions of without containing Li^+, symmetric redox peaks do not appear, demonstrating the excellent selectivity of SnLMO-1 for Li^+. Additionally, in solutions containing Li^+, two plateaus appear in the constant current discharge curves, corresponding to the two-step intercalation/deintercalation reaction of Li^+. Na^+, K^+, and Ca^{2+} experience steric hindrance, making it difficult for them to enter the tetrahedral sites of λ-MnO_2.[40] Additionally, hydrated Mg^{2+} has a higher dehydration energy and requires two nucleation sites for insertion.[41] These factors contribute to the selective intercalation of Li^+ into LMO.

However, compared to the LiCl solution, the presence of cations such as Na^+, K^+, Mg^{2+}, and Ca^{2+} in a solution affects the electrochemical behavior of Li^+. The redox voltage in the CV curve is mainly influenced by the Li^+ migration channel in LMO.[42] The current in the CV curve is determined by the amount of Li^+ inserted into the structure, which is governed by the transport properties of the lithium-ion channels.[43] The shifts in peak voltages, therefore, can be attributed to changes in the ion transport dynamics, particularly due to the interference of additional cations in the electrolyte. A small amount of Na^+, K^+, Mg^{2+}, and Ca^{2+} ions can adsorb

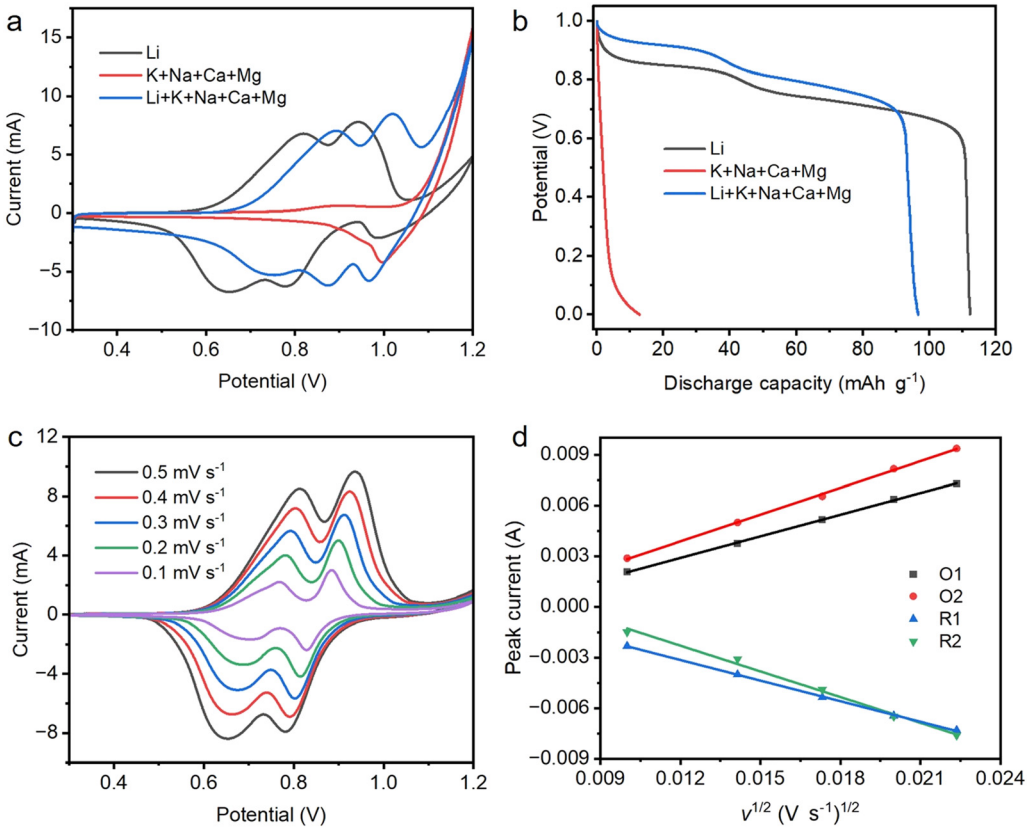

Fig. 3 Cyclic voltammograms curve (a) and discharge curves (b) of SnLMO-1 in different electrolytes; cyclic voltammograms curve of SnLMO-1 in different scan rate (c); linear relationship between $v^{1/2}$ and corresponding with redox peak current (d).

onto the lithium-ion migration channels of LMO, hindering the insertion of Li^+.[44] This adsorption effect can increase the reduction potential (or discharge voltage), as seen in Fig. 3a, S6 and S7.† These ions occupy part of the space in the migration channels, making it more difficult for Li^+ to diffuse and intercalate into the material, thus leading to an increase in the reduction voltage.[45] Additionally, the presence of cations in the electrolyte also affects the electric field distribution at the electrode/electrolyte interface, which can lead to electrochemical polarization. This polarization affects the extraction of Li^+, resulting in an increase in the oxidation potential.[46] In summary, the observed shifts in the CV curves are primarily due to the combined effects of ionic competition in the migration channels and the electrochemical polarization caused by the cations.

2.2.2 Electrochemical dynamics. The study explored the influence of scan rate on the redox processes of SnLMO and LMO electrodes in a LiCl (lithium chloride) solution using cyclic voltammetry (Fig. 3c, d, and S8†). As the scan rate increased, both the oxidation and reduction peak currents increased as well. Additionally, the oxidation peak potential shifted to higher values, and the reduction peak potential moved to lower values. These shifts indicate that the processes involving the capture and release of Li^+ in the SnLMO and LMO electrodes are controlled by kinetic factors.[47] The oxidation and reduction peak currents show a linear relationship with $v^{1/2}$, suggesting that the electrode surface processes are predominantly diffusion-controlled.[48,49] The diffusion coefficients calculated by Randles–Sevcik equation ($I_p = (2.69 \times 10^5)n^{3/2}AD^{1/2}v^{1/2}C_0$), where I_p is peak current, n is number of electrons, A is effective area of the electrode in cm^2, D is chemical diffusion coefficient of active materials in $cm^2\ s^{-1}$, v is scan rate in V s^{-1}, and C_0 is bulk phase concentration in mol cm^{-3}.[41] The linear equation and correlation coefficient between I_p and $v^{1/2}$ are shown in Table S1.† The researchers calculated the D of Li^+ for the redox reactions of the electrodes, with the results summarized in Table 1. The Li^+ diffusion coefficient of SnLMO-1 is superior to that of LMO, SnLMO-2, and SnLMO-3, due to the favorable diffusion of Li^+ by SnO_2 nanoparticles, while SnO_2 nanowires hinder the diffusion of Li^+.[50] This indicates that the morphology and structure of the electrode materials significantly impact their electrochemical performance. The impedance values for the different samples were measured as follows: SnLMO-1 < SnLMO-3 < SnLMO-2 < LMO (Fig. S9†). In LMO modified with nanowires, Li^+ must travel longer distances to reach the active material and withstand greater charge and discharge stresses.[51] This longer diffusion path leads to increased resistance and slower kinetics during charging and discharging, reducing the overall performance compared to nanoparticles where the active material is readily accessible. While SnLMO-3 contains a substantial

Table 1 Li^+ diffusion coefficients of LMO and SnLMO (unit: $cm^2\ s^{-1}$)

D_{Li^+}	O_1	O_2	R_1	R_2	Average
LMO	5.02×10^{-12}	6.85×10^{-12}	2.93×10^{-12}	4.81×10^{-12}	4.90×10^{-12}
SnLMO-1	8.92×10^{-12}	1.36×10^{-11}	8.14×10^{-12}	1.27×10^{-11}	1.08×10^{-11}
SnLMO-2	5.98×10^{-12}	1.10×10^{-11}	6.02×10^{-12}	1.13×10^{-11}	8.58×10^{-12}
SnLMO-3	4.81×10^{-12}	8.13×10^{-12}	4.15×10^{-12}	8.02×10^{-12}	6.28×10^{-12}

number of nanowires, which also aids in enhancing electron transfer, the improvement in conductivity is not as significant as that observed in the nanoparticle-loaded LMO. The trend in impedance values is consistent with the trends in Li^+ diffusion, both demonstrating that SnO_2 nanoparticle modification of LMO (SnLMO-1) can effectively enhance the electrochemical performance for lithium extraction.

2.3 The mechanism of the lithium deintercalation process

To study the mechanism of Li^+ extraction selectivity of SnLMO-1, the structural characteristics of electrode materials at different potentials during charging and discharging processes were analyzed. Previous literature has indicated that under the influence of an electric field, LMO may undergo reactions represented by reactions (1) and (2) with Li^+.[52,53] Additionally, in a LiCl solution, charging and discharging were conducted within the range of 0–1.0 V at a current density of 50 mA g^{-1}, and the corresponding XRD profiles at the respective voltages are shown in Fig. 4. During charging, with increasing potential, the (111) crystal plane of SnLMO-1 shifted towards higher angles (from 18.84° to 19.06°), indicating a decrease in lattice spacing, transforming the electrode material from SnLMO-1 to SnO_2–λ-MnO_2.[54] During discharging, with decreasing potential, the (111) crystal plane of SnLMO-1 shifted towards lower angles (from 19.06° to 18.64°). After completing one cycle, the characteristic peaks of the (111) crystal plane return to their initial positions, indicating the reversible deintercalation of Li^+. This reversible change demonstrates the structural stability and efficiency of SnLMO-1 as an electrode material for lithium extraction, highlighting its potential application in lithium recovery.

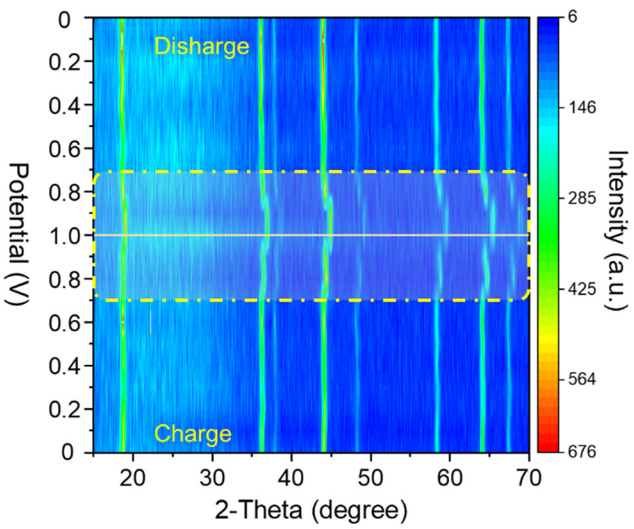

Fig. 4 The quasi *in situ* Raman spectral contour plot of SnLMO-1.

$$2LiMn_2O_4 \rightleftharpoons 2Li_{0.5}Mn_2O_4 + Li^+ + e^- \quad (1)$$

$$2Li_{0.5}Mn_2O_4 \rightleftharpoons 4\lambda\text{-}MnO_2 + Li^+ + e^- \quad (2)$$

2.4 Performance

We studied the cycling performance of SnLMO with different modified amounts in a 30 mL of 1.0 mol L^{-1} LiCl (three-electrode system, current density of 50 mA g^{-1}), as shown in Fig. 5a. After 30 cycles, the capacity retention rates of LMO, SnLMO-1, SnLMO-2, and SnLMO-3 were 36.52%, 61.03%, 55.83%, and 30.45%, respectively. The specific surface area of the material has a significant impact on the lithium extraction capacity. The N_2 isothermal adsorption curve results show that the specific surface areas of LMO, SnLMO-1, SnLMO-2, and SnLMO-3 are 1.9, 4.3, 9.1, and 13.3 $cm^2\ g^{-1}$, respectively (Fig. S10†). Due to the increased specific surface area of SnO_2 nanowires loaded, SnLMO-3 exhibited better discharge capacity than other materials in the first 15 cycles. However, it experienced significant decay after 15 cycles, possibly due to volume expansion of SnO_2 nanowires upon lithiation, leading to poor reversible cycling performance.[52] Modification of SnO_2 nanoparticles into island-like structures is beneficial for reducing the stress of LMO (SnLMO-1) during redox reaction processes and enhancing the surface area, thereby enhancing the material's cycling stability. Additionally, the dissolution of Mn in the electrolyte after cycling was examined, with results shown in Fig. 5b. In LiCl electrolyte, during the SnLMO and LMO redox reaction processes, partial Mn^{3+} underwent disproportionation reactions (Jahn–Teller effect), generating soluble Mn^{2+} that dissolved and diffused into the electrolyte.[55] The R_{Mn} in SnLMO-1 was 0.14%, lower than that of LMO (0.16%), SnLMO-2 (0.15%), and SnLMO-3 (0.16%). This indicates that modified SnO_2 nanoparticles can reduce stress on the electrode surface during $Mn^{3+/4+}$ redox reaction processes and suppress the occurrence of the Jahn–Teller effect. Furthermore, through XRD spectra of electrode materials before and after cycling, it was observed that SnLMO-1 exhibited a low-angle shift after the first cycle (attributed to electrode activation during the first charge–discharge cycle), and the characteristic peaks at the 5th, 10th, 15th, and 30th

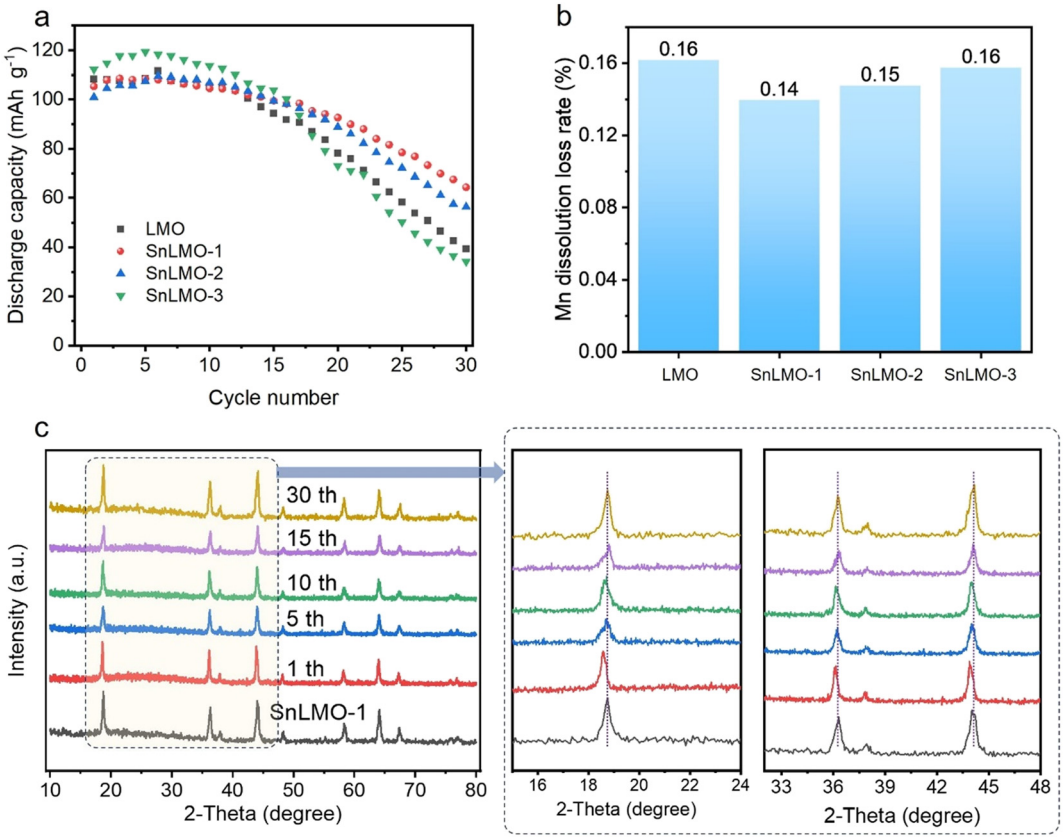

Fig. 5 Cycling performance (a) and Mn dissolution loss rate R_{Mn} (b) of LMO and SnLMO; XRD patterns of SnLMO-1 cycling process (c).

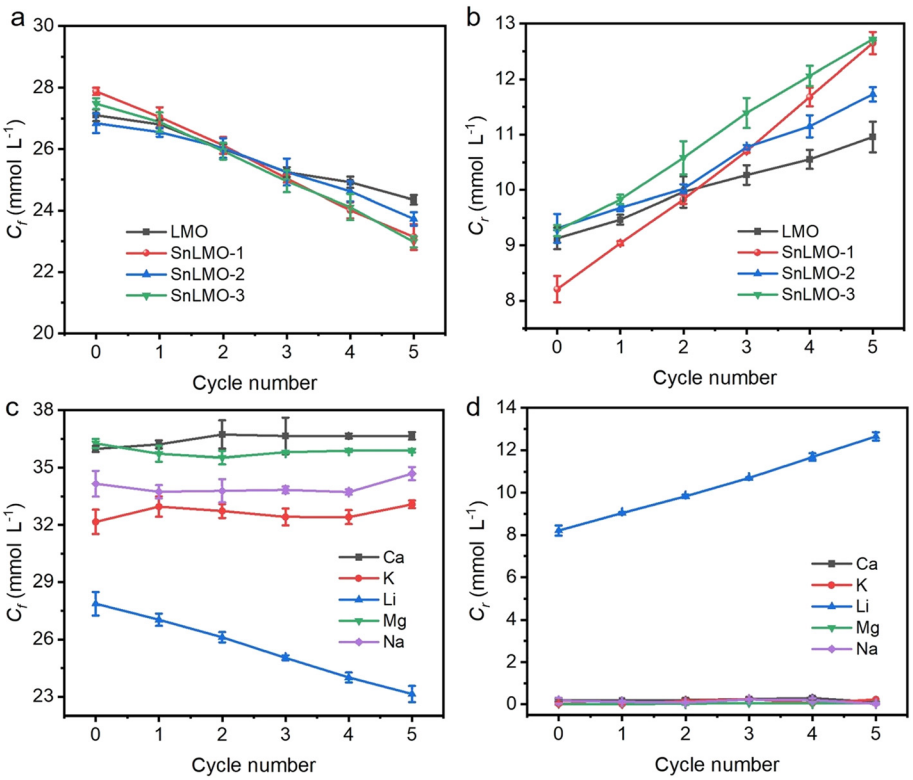

Fig. 6 Concentration changes of Li^+ in feed solution (a), corresponding recovery solution (b), simulated brine (c), and corresponding recovery solution (d) during lithium intercalation or deintercalation.

Table 2 Comparison of lithium extraction performance of different electrode materials

Electrochemical system	Purity (%)	Capacity (mg g^{-1})	Ref.
LMO//PPy	—	4.43	56
NCM//Ag	96.4	10.83	57
LMNC//Bi	92.5	13.05	58
LMO//AEM//MnO_2	—	22	44
LNMM//AC	97.2	14.4	59
rGO/NCM//AC	93.4	13.84	60
α-$LiAlO_2$//AC	—	8.25	61
LMO//$Li_{1-x}Mn_2O_4$	—	17.20	48
PPy/Al_2O_3/LMO//AC	97.4	12.84	41
HTO/rGO-TA//AC	—	25.2	62
SnLMO-1//Ag	96.9	19.76	This work

PPy: polypyrrole; NCM: $Li_{1-x}Ni_{0.33}Co_{1/3}Mn_{1/3}O_2$; LMNC: $Li_{1.16}Mn_{0.6}Ni_{0.12}Co_{0.12}O_2$; LNMM: $LiNi_{0.038}Mo_{0.012}Mn_{1.95}O_4$; rGO/NCM: graphene-coated $LiNi_{0.6}Co_{0.2}Mn_{0.2}O_2$; HTO/rGO-TA: H_2TiO_3/reduced graphene oxide–tannic acid.

cycles remained consistent with the initial state, indicating its excellent cycling stability (Fig. 5c), demonstrating good chemical stability of the composite material.

The study evaluates the lithium recovery performance of LMO and SnLMO in a simulated brine solution containing 30 mmol L^{-1} concentrations of various chloride salts (LiCl, NaCl, KCl, $MgCl_2$, and $CaCl_2$) using electrochemical methods (Fig. 6a and b). The performance was measured over five capture and release cycles. The average extraction capacities of LMO, SnLMO-1, SnLMO-2, and SnLMO-3 were 11.45, 19.76, 17.97, and 18.76 mg g^{-1}, respectively; and the average release capacities were 7.61, 18.45, 10.77, and 14.36 mg g^{-1}, respectively. The results indicate that SnO_2 modified LMO can increase Li^+ adsorption capacity, attributed to larger specific surface area and smaller electron transfer resistance. Further, when utilizing the SnLMO-1//Ag electrochemical system for lithium extraction from the mixed chloride solution, the average extraction and release capacities were 19.76 and 18.45 mg g^{-1}, respectively, after five cycles (Fig. 6c). The system also demonstrated minimal changes in other cations within the solution and achieved a lithium purity of 96.90% in the recovery solution (Fig. 6d). Compared with previous studies (Table 2), SnLMO-1 exhibits good selectivity and extraction capacity, attributed to SnO_2 as an excellent lithium storage material effectively increasing lithium ion extraction capacity, and Ag demonstrating good reversibility to the electrode.

3 Conclusion

This work designs lithium storage type metal oxide SnO_2 island-modified LMO electrode materials, endowing them with high Li^+ diffusion capability and electro-adsorption capacity. The electro-adsorption capacity in simulated brine (210 mg L^{-1} Li^+) is 19.76 mg g^{-1}, the Li^+ diffusion coefficient is 1.08×10^{-11} cm^2 s^{-1}, and the capacity retention rate after 30 cycles is 61.03%, which is higher than that of unmodified LMO. However, SnO_2 nanowire-modified LMO exhibits a higher initial discharge capacity but poor cycling stability (30-cycle capacity retention rate of 30.45%). Therefore, SnO_2 nanoparticle modification has better stability than nanowires, attributed to the island modification of nanoparticles reducing the stress generated during the charge–discharge process, and suppressing the distortion of electrode material structure.

Data availability

Data will be made available on request.

Conflicts of interest

The authors declare no conflict of interest.

Acknowledgements

This work was supported by the National Key R&D Program of China (No. 2022YFE0208300), the National Natural Science Foundation of China (No. 22278426 and 21908082), the Science Foundation of China University of Petroleum, Beijing (No. 2462024XKBH001, 2462022YJRC003, 2462022YJRC002).

References

1 Y. Song, S. Fang, N. Xu, M. Wang, S. Chen, J. Chen, B. Mi and J. Zhu, Solar transpiration–powered lithium extraction and storage, *Science*, 2024, **385**, 1444–1449.
2 Z. Li, I.-C. Chen, L. Cao, X. Liu, K.-W. Huang and Z. Lai, Lithium extraction from brine through a decoupled and membrane-free electrochemical cell design, *Science*, 2024, **385**, 1438–1444.
3 S. Zavahir, T. Elmakki, M. Gulied, Z. Ahmad, L. Al-Sulaiti, H. K. Shon, Y. Chen, H. Park, B. Batchelor and D. S. Han, A review on lithium recovery using electrochemical capturing systems, *Desalination*, 2021, **500**, 114883.
4 P. K. Choubey, M.-S. Kim, R. R. Srivastava, J.-C. Lee and J.-Y. Lee, Advance review on the exploitation of the prominent energy-storage element: Lithium. Part I: From mineral and brine resources, *Miner. Eng.*, 2016, **89**, 119–137.
5 Y. Zhang, W. Sun, R. Xu, L. Wang and H. Tang, Lithium extraction from water lithium resources through green

electrochemical-battery approaches: A comprehensive review, *J. Cleaner Prod.*, 2021, **285**, 124905.
6 G. Zhou, X. Li, L. Chen, G. Luo, J. Gu, J. Zhu, J. Yu, J. Yin, Y. Chao and W. Zhu, Construction of porous disc-like lithium manganate for rapid and selective electrochemical lithium extraction from brine, *Chin. J. Chem. Eng.*, 2023, **54**, 316–322.
7 G. Zhou, L. Chen, X. Li, G. Luo, Z. Yu, J. Yin, L. Fan, Y. Chao, L. Jiang and W. Zhu, Construction of truncated-octahedral $LiMn_2O_4$ for battery-like electrochemical lithium recovery from brine, *Green Energy Environ.*, 2023, **8**, 1081–1090.
8 J. Yu, J. Zhu, G. Luo, L. Chen, X. Li, P. Cui, P. Wu, Y. Chao, W. Zhu and Z. Liu, 3D-printed titanium-based ionic sieve monolithic adsorbent for selective lithium recovery from salt lakes, *Desalination*, 2023, **560**, 116651.
9 T. Ding, M. Zheng, S. Peng, Y. Lin, X. Zhang and M. Li, Lithium extraction from salt lakes with different hydrochemical types in the Tibet Plateau, *Geosci. Front.*, 2023, **14**, 101485.
10 P. Xu, J. Hong, X. Qian, Z. Xu, H. Xia, X. Tao, Z. Xu and Q. Ni, Materials for lithium recovery from salt lake brine, *J. Mater. Sci.*, 2020, **56**, 16–63.
11 R. Bagheri, M. Ghaedi, A. Asfaram, E. Alipanahpour Dil and H. Javadian, RSM-CCD design of malachite green adsorption onto activated carbon with multimodal pore size distribution prepared from Amygdalus scoparia: Kinetic and isotherm studies, *Polyhedron*, 2019, **171**, 464–472.
12 X. Li, Y. Chao, L. Chen, W. Chen, J. Luo, C. Wang, P. Wu, H. Li and W. Zhu, Taming wettability of lithium ion sieve via different TiO_2 precursors for effective Li recovery from aqueous lithium resources, *Chem. Eng. J.*, 2020, **392**, 123731.
13 A. Battistel, M. S. Palagonia, D. Brogioli, F. La Mantia and R. Trocoli, Electrochemical methods for lithium recovery: A comprehensive and critical review, *Adv. Mater.*, 2020, **32**, e1905440.
14 W. Yu, Y. Wang, A. Wu, A. Li, Z. Qiu, X. Dong, C. Dong and H. Huang, Suppress oxygen evolution of lithium-rich manganese-based cathode materials via an integrated strategy, *Green Energy Environ.*, 2024, **9**, 138–151.
15 H. Joo, J. Lee and J. Yoon, Short Review: Timeline of the electrochemical lithium recovery system using the spinel $LiMn_2O_4$ as a positive electrode, *Energies*, 2020, **13**, 6235.
16 J. Wang, X. Yue, P. Wang, T. Yu, X. Du, X. Hao, A. Abudula and G. Guan, Electrochemical technologies for lithium recovery from liquid resources: A review, *Renewable Sustainable Energy Rev.*, 2022, **154**, 111813.
17 B. Hu, X. Shang, P. Nie, B. Zhang, J. Yang and J. Liu, Lithium ion sieve modified three-dimensional graphene electrode for selective extraction of lithium by capacitive deionization, *J. Colloid Interface Sci.*, 2022, **612**, 392–400.
18 K. T. Kubra, M. S. Salman, M. N. Hasan, A. Islam, S. H. Teo, M. M. Hasan, M. C. Sheikh and M. R. Awual, Sustainable detection and capturing of cerium(III) using ligand embedded solid-state conjugate adsorbent, *J. Mol. Liq.*, 2021, **338**, 116667.
19 R. Trócoli, A. Battistel and F. L. Mantia, Selectivity of a lithium-recovery process based on $LiFePO_4$, *Chemistry*, 2014, **20**, 9888–9891.
20 M. N. Hasan, M. A. Shenashen, M. M. Hasan, H. Znad and M. R. Awual, Assessing of cesium removal from wastewater using functionalized wood cellulosic adsorbent, *Chemosphere*, 2021, **270**, 128668.
21 X. Jia, M. Hu, K. Soundarapandian, X. Yu, Z. Liu, Z. Chen, A. Narita, K. Mullen, F. H. L. Koppens, J. Jiang, K. J. Tielrooij, M. Bonn and H. I. Wang, Kinetic ionic permeation and interfacial doping of supported graphene, *Nano Lett.*, 2019, **19**, 9029–9036.
22 K. Hayamizu, Y. Chiba and T. Haishi, Dynamic ionic radius of alkali metal ions in aqueous solution: A pulsed-field gradient NMR study, *RSC Adv.*, 2021, **11**, 20252–20257.
23 B. Tansel, Significance of thermodynamic and physical characteristics on permeation of ions during membrane separation: Hydrated radius, hydration free energy and viscous effects, *Sep. Purif. Technol.*, 2012, **86**, 119–126.
24 Y. Gu, K. Yang, H. Yao, W. Li, H. Zhan, X. Ming, G. Huang, G. Li and F. Zhan, Surface modification of Li_3InCl_6 provides superior electrochemical performance for $LiMn_2O_4$ cathode materials, *Chin. Chem. Lett.*, 2023, **34**, 108047.
25 G. Luo, M. Zhou, Y. Chao, P. Cui, X. Li, L. Chen, G. Jiang, W. Zhu, Z. Liu and C. Xu, Augmented electrochemical extraction lithium performance via interface alloying modification, *Sep. Purif. Technol.*, 2025, **354**, 128683.
26 C. P. Lawagon, G. M. Nisola, R. A. I. Cuevas, R. E. C. Torrejos, H. Kim, S. P. Lee and W. J. Chung, Li $Ni_{0.5}Mn_{1.5}O_4$/Ag for electrochemical lithium recovery from brine and its optimized performance via response surface methodology, *Sep. Purif. Technol.*, 2019, **212**, 416–426.
27 Y. Sun, Y. Wang, Y. Liu and X. Xiang, Highly efficient lithium extraction from brine with a high sodium content by adsorption-Coupled electrochemical technology, *ACS Sustainable Chem. Eng.*, 2021, **9**, 11022–11031.
28 Z. Zhang, X. Du, Q. Wang, F. Gao, T. Jin, X. Hao, P. Ma, J. Li and G. Guan, A scalable three-dimensional porous λ-MnO_2/rGO/Ca-alginate composite electroactive film with potential-responsive ion-pumping effect for selective recovery of lithium ions, *Sep. Purif. Technol.*, 2021, **259**, 118111.
29 G. Luo, L. Zhu, X. Li, G. Zhou, J. Sun, L. Chen, Y. Chao, L. Jiang and W. Zhu, Electrochemical lithium ions pump for lithium recovery from brine by using a surface stability Al_2O_3–ZrO_2 coated $LiMn_2O_4$ electrode, *J. Energy Chem.*, 2022, **69**, 244–252.
30 Y. Wang, J. Zhang, Z. Cheng and X. Xiang, Hydrophilic modification using polydopamine on core–shell $Li_{1.6}Mn_{1.6}O_4$@Carbon electrodes for lithium extraction from lake brine, *ACS Sustainable Chem. Eng.*, 2022, **10**, 8970–8979.
31 T. Song and U. Paik, TiO_2 as an active or supplemental material for lithium batteries, *J. Mater. Chem. A*, 2016, **4**, 14–31.
32 T. L. Nguyen, J. Hur and I. T. Kim, Facile Synthesis of quantum dots SnO_2/Fe_3O_4 hybrid composites for superior reversible lithium-ion storage, *J. Ind. Eng. Chem.*, 2019, **72**, 504–511.
33 T. P. Nguyen and I. T. Kim, Self-assembled few-layered MoS_2 on SnO_2 anode for enhancing lithium-ion storage, *Nanomaterials*, 2020, **10**, 2558.

34 J. Li, Y. Zhao, N. Wang and L. Guan, A high performance carrier for SnO_2 nanoparticles used in lithium ion battery, *Chem. Commun.*, 2011, **47**, 5238.

35 Y. Lee, T. Y. Kim, D.-W. Kim, J. K. Lee and W. Choi, Coating of spinel $LiNi_{0.5}Mn_{1.5}O_4$ cathodes with SnO_2 by an electron cyclotron resonance metal–organic chemical vapor deposition method for high-voltage applications in lithium ion batteries, *J. Electroanal. Chem.*, 2015, **736**, 16–21.

36 Y. Chen, W. Qin, J. An, J. Zhang and X. Wen, Island-like MoO_{3-x} film grown on Mo foil as high-performance lithium-ion battery anode: a new strategy for preparing flexible electrode, *J. Mater. Sci.*, 2022, **57**, 5552–5565.

37 F. Lv, H. Cheng, W. Nie, Q. Sun, Y. Liu, T. Duan, Q. Xu and X. Lu, Enhancing rate capacity and cycle stability of $LiNi_{1/3}Co_{1/3}Mn_{1/3}O_2$ cathode material by laminar V_2O_5 coating for lithium-ion batteries, *ChemistrySelect*, 2021, **6**, 6339–6347.

38 Z. Wang, T. Han, T. Fei, S. Liu and T. Zhang, Investigation of microstructure effect on NO_2 sensors based on SnO_2 nanoparticles/reduced graphene oxide hybrids, *ACS Appl. Mater. Interfaces*, 2018, **10**, 41773–41783.

39 S. Wang, C. Luo, Y. Feng, G. Fan, L. Feng, M. Ren and B. Liu, Electrochemical properties and microstructures of $LiMn_2O_4$ cathodes coated with aluminum zirconium coupling agents, *Ceram. Int.*, 2020, **46**, 13003–13013.

40 N. Xie, Y. Li, Y. Lu, J. Gong and X. Hu, Electrochemically controlled reversible lithium capture and release enabled by $LiMn_2O_4$ nanorods, *ChemElectroChem*, 2019, **7**, 105–111.

41 X. Zhao, Y. Jiao, P. Xue, M. Feng, Y. Wang and Z. Sha, Efficient lithium extraction from brine using a three-dimensional nanostructured hybrid inorganic-gel framework electrode, *ACS Sustainable Chem. Eng.*, 2020, **8**, 4827–4837.

42 H. Fu, W. Xu, Z. Yu, L. He and Z. Zhao, Identifying electrochemical performance of $LiFePO_4$ with different exposed crystal facets for voltammetric determination of Li^+, *J. Electroanal. Chem.*, 2024, **973**, 118672.

43 W. Xu, L. He and Z. Zhao, Lithium extraction from high Mg/Li brine via electrochemical intercalation/de-intercalation system using $LiMn_2O_4$ materials, *Desalination*, 2021, **503**, 114935.

44 M. Zhao, Z. Ji, Y. Zhang, Z. Guo, Y. Zhao, J. Liu and J. Yuan, Study on lithium extraction from brines based on $LiMn_2O_4$/$Li_{1-x}Mn_2O_4$ by electrochemical method, *Electrochim. Acta*, 2017, **252**, 350–361.

45 D. F. Liu, S. Y. Sun and J. G. Yu, Electrochemical and adsorption behaviour of Li^+, Na^+, K^+, Ca^{2+}, and Mg^{2+} in $LiMn_2O_4$/λ-MnO_2 structures, *Can. J. Chem. Eng.*, 2018, **97**, 1589–1595.

46 M. Kunitski, N. Eicke, P. Huber, J. Kohler, S. Zeller, J. Voigtsberger, N. Schlott, K. Henrichs, H. Sann, F. Trinter, L. P. H. Schmidt, A. Kalinin, M. S. Schoffler, T. Jahnke, M. Lein and R. Dorner, Double-slit photoelectron interference in strong-field ionization of the neon dimer, *Nat. Commun.*, 2019, **10**, 1.

47 B. Liu, B. Xiao, L. Cui and M. Wang, Molecularly imprinted electrochemical sensor for the highly selective and sensitive determination of melamine, *Mater. Sci. Eng., C*, 2015, **55**, 457–461.

48 D. Liu, W. Xu, J. Xiong, L. He and Z. Zhao, Electrochemical system with $LiMn_2O_4$ porous electrode for lithium recovery and its kinetics, *Sep. Purif. Technol.*, 2021, **270**, 118809.

49 Y. Mu, C. Zhang, W. Zhang and Y. Wang, Electrochemical lithium recovery from brine with high Mg^{2+}/Li^+ ratio using mesoporous λ-MnO_2/$LiMn_2O_4$ modified 3D graphite felt electrodes, *Desalination*, 2021, **511**, 115112.

50 C. Kim, M. Noh, M. Choi, J. Cho and B. Park, Critical size of a nano SnO_2 electrode for Li-secondary battery, *Chem. Mater.*, 2005, **17**, 3297–3301.

51 H. Wang, X. Shan, H. Yu, Y. Wang, W. Schmickler, H. Y. Chen and N. Tao, Determining electrochemical surface stress of single nanowires, *Angew. Chem., Int. Ed.*, 2017, **56**, 2132–2135.

52 S. Zhao, C. D. Sewell, R. Liu, S. Jia, Z. Wang, Y. He, K. Yuan, H. Jin, S. Wang, X. Liu and Z. Lin, SnO_2 as advanced anode of alkali-ion batteries: Inhibiting Sn coarsening by crafting robust physical barriers, void boundaries, and heterophase interfaces for superior electrochemical reaction reversibility, *Adv. Energy Mater.*, 2019, **10**, 1902657.

53 X. Xu, Y. Zhou, Z. Feng, N. U. Kahn, Z. U. Haq Khan, Y. Tang, Y. Sun, P. Wan, Y. Chen and M. Fan, A self-supported lambda-MnO_2 film electrode used for electrochemical lithium recovery from brines, *ChemPlusChem*, 2018, **83**, 521–528.

54 G. Luo, X. Li, L. Chen, Y. Zhang, J. Gu, Y. Chao, W. Zhu, Z. Liu and C. Xu, Island-like CeO_2 decorated $LiMn_2O_4$: Surface modification enhancing electrochemical lithium extraction and cycle performance, *Chem. Eng. J.*, 2023, **455**, 140928.

55 C. Zuo, Z. Hu, R. Qi, J. Liu, Z. Li, J. Lu, C. Dong, K. Yang, W. Huang, C. Chen, Z. Song, S. Song, Y. Yu, J. Zheng and F. Pan, Double the capacity of manganese spinel for lithium-ion storage by suppression of cooperative Jahn–Teller distortion, *Adv. Energy Mater.*, 2020, **10**, 2000363.

56 L. L. Missoni, F. Marchini, M. í. D. Pozo and E. J. Calvo, A $LiMn_2O_4$-polypyrrole system for the extraction of LiCl from natural brine, *J. Electrochem. Soc.*, 2016, **163**, A1898–A1902.

57 C. P. Lawagon, G. M. Nisola, R. A. I. Cuevas, H. Kim, S. P. Lee and W. J. Chung, $Li_{1-x}Ni_{0.33}Co_{1/3}Mn_{1/3}O_2$/Ag for electrochemical lithium recovery from brine, *Chem. Eng. J.*, 2018, **348**, 1000–1011.

58 X. Zhao, H. Yang, Y. Wang, L. Yang and L. Zhu, Lithium extraction from brine by an asymmetric hybrid capacitor composed of heterostructured lithium-rich cathode and nano-bismuth anode, *Sep. Purif. Technol.*, 2021, **274**, 119078.

59 X. Zhao, G. Li, M. Feng and Y. Wang, Semi-continuous electrochemical extraction of lithium from brine using CF-NMMO/AC asymmetric hybrid capacitors, *Electrochim. Acta*, 2020, **331**, 135285.

60 X. Zhao, M. Feng, Y. Jiao, Y. Zhang, Y. Wang and Z. Sha, Lithium extraction from brine in an ionic selective desalination battery, *Desalination*, 2020, **481**, 114360.

61 T. Elmakki, S. Zavahir, U. Hafsa, L. Al-Sulaiti, Z. Ahmad, Y. Chen, H. Park, H. K. Shon, Y. C. Ho and D. S. Han, Novel $LiAlO_2$ material for scalable and facile lithium recovery using electrochemical ion pumping, *Nanomaterials*, 2023, **13**, 895.

62 J. Zhang, Z. Cheng, X. Qin, X. Gao, R. Yun and X. Xiang, Bifunctional modification enhances lithium extraction from brine using a titanium-based ion sieve membrane electrode, *ACS Appl. Mater. Interfaces*, 2023, **15**, 29586–29596.